JOURNAL OF THEORETICAL AND APPLIED MECHANICS
46, 3, pp. 641-664, Warsaw 2008

CONTROL AND CHAOS FOR VIBRO-IMPACT AND NON-IDEAL OSCILLATORS

Silvio L.T. de Souza
Iberê L. Caldas

University of São Paulo, Institute of Physics, São Paulo, SP, Brazil
e-mail: thomaz@if.usp.br; ibere@if.usp.br

Ricardo L. Viana

Federal University of Paraná, Departament of Physics, Curitiba, PR, Brazil
e-mail: viana@fisica.ufpr.br

José M. Balthazar

State University of São Paulo, Department of Statistics, Computational and Applied Mathematics, Rio Claro, SP, Brazil; e-mail: jmbaltha@rc.unesp.br

In the paper, we discuss dynamics of two kinds of mechanical systems. Initially, we consider vibro-impact systems which have many implementations in applied mechanics, ranging from drilling machinery and metal cutting processes to gear boxes. Moreover, from the point of view of dynamical systems, vibro-impact systems exhibit a rich variety of phenomena, particularly chaotic motion. In this paper, we review recent works on the dynamics of vibro-impact systems, focusing on chaotic motion and its control. The considered systems are a gear-rattling model and a smart damper to suppress chaotic motion. Furthermore, we investigate systems with non-ideal energy source, represented by a limited power supply. As an example of a non-ideal system, we analyse chaotic dynamics of the damped Duffing oscillator coupled to a rotor. Then, we show how to use a tuned liquid damper to control the attractors of this non-ideal oscillator.

Key words: vibro-impact, chaos, control of chaos, non-ideal oscillators

1. Introduction

There is a steadfast interest in the theoretical and experimental study of vibro-impact systems which have oscillating parts colliding with other vibrating components or rigid walls (Blazejczyk-Okolewska *et al.*, 2004). Vibro-impact systems are widely found in engineering applications, like vibration

hammers, drilling machinery, milling, impact print hammers, and shock absorbers (Blazejczyk-Okolewska *et al.*, 1999). There are also undesirable effects coming from vibro-impact systems like gearboxes, bearings, and fuel elements in nuclear reactors: large amplitude response leading to material fatigue and rattling (Jerrelind and Stensson, 2000).

From the point of view of dynamical systems, however, vibro-impact systems are extremely rich models, for they exhibit a wealth of phenomena like bifurcations, chaos, crises, multi-stability, and final state sensitivity (Peterka and Vacik, 1992; Ivanov, 1996; Wiercigroch and de Kraker, 2000). The distinctive dynamical character of vibro-impact systems is their non-smoothness due to impacts with several types of amplitude constraints (Nordmark, 1991; Luo, 2004; Luo *et al.*, 2006, 2007). In this case, the impacts are treated by modifying the initial conditions of motions according to an impact rule considering the coefficient of restitution. Another interesting and useful approach is to introduce piecewise stiffness characteristics for describing impacting systems (Wiercigroch, 2000; Ing *et al.*, 2006; de Souza *et al.*, 2007c).

Another key issue related to the dynamics of vibro-impact systems is the control of their oscillations (Kapitaniak, 2000). In fact, chaotic oscillations, being intrinsically random and unpredictable, are generally considered as an undesirable, even harmful phenomenon when it occurs. Hence the control of chaos in vibro-impact systems has immediate practical applications as, e.g. the suppression of rattling noise in gearboxes (Karagiannis and Pfeiffer, 1991).

Several other important features of impact oscillators with practical applications have also been analysed. Thus, impacts are also employed to describe step disturbances in multi-body mechanical systems of many industrial machines (Czolczynski *et al.*, 2000). Moreover, instabilities and bifurcations have been explained by considering impact systems with bounded progressive motions (drifts) (Pavlovskaia *et al.*, 2001) or low-velocity collisions causing the so called grazing effect (Nordmark, 1991). Another relevant application comes from considering impact systems with dry friction generating high amplitude forces involving dynamic fractures required to drilling brittle materials (Wiercigroch *et al.*, 2005).

In this paper an overview of the modern research on vibro-impact systems dynamics, focusing on chaos and its control is presented. We shall briefly present each model and how to derive its governing equations from first principles. We shall present dynamical features like phase portraits, bifurcation diagrams, Lyapunov exponents, and basin boundaries, including quantitative characterisations of chaotic motion and final state sensitivity (fractal basin boundaries).

The above mentioned works deal with oscillators that are driven by systems whose amplitude and frequency can be arbitrarily chosen. However, in several mechanical experiments this cannot be achieved because the forcing source has a limited available energy supply. This has been called non-ideal energy sources (Kononenko, 1969). A common example appears when the driving comes from an unbalanced rotor linked to the oscillator. As a consequence of this mechanical coupling, the rotor dynamics may be heavily influenced by the oscillating system being forced. As a consequence, the resulting oscillations differ from those predicted for experiments with ideal energy sources. Hence, the driven system cannot be considered as given a priori, but it must be taken also as a consequence of the dynamics of the whole system (oscillator plus rotor) (Dimentberg *et al.*, 1997; de Souza *et al.*, 2005a, 2007b).

This paper is organized as follows: Section 2 deals with a single-stage gearbox system under periodic excitation. Section 3 considers a simple model of vibro-impact system consisting of a linear oscillator undergoing inelastic collisions with a fixed barrier. We study the suppression of chaotic motion by a smart damper which changes the damping coefficient according to the sign of the relative velocity. A non-ideal oscillator is treated in Section 4, where a damped Duffing oscillator is coupled to a non-ideal motor driving a rotor. This procedure introduces more degrees of freedom in the system, but it turns out to be a more realistic model of a finite-power external source of driving to the system. Section 5 combines such a non-linear oscillator with a U-tube filled with liquid as the damping mechanism. Our conclusions are left to the last Section.

2. Gear-box system

Gear units have typically backlashes or variable clearances between adjacent moving parts, and these backlashes need to allow thermal expansion and lubrification of the moving wheels. The presence of backlashes makes gear teeth to lose contact for a short interval generating repeated collisions and a hammering effect (Pfeiffer and Kunert, 1990). In spur gears of engines driving camshafts and injection pump shafts, for example, rattling is the source of uncomfortable noise. Hence, many theoretical and experimental efforts have been devoted to the understanding of such vibro-impact problems (Karagiannis and Pfeiffer, 1991).

2.1. Gear-rattling model

We focus on the gearbox rattling model proposed by Pfeiffer and collaborators, and consisting of two spur gears with different diameters and a gap between the teeth (single-stage rattling) (de Souza and Caldas, 2001), Fig. 1. Motion of one gear is supposed to be sinusoidal the with well-defined amplitude and frequency, whereas motion of the other gear results from the system dynamics. The gears have radii R and R_e, and a backlash ν between the teeth. Motion of the driving wheel is described by a harmonic function $e(t) = -A\sin(\omega t)$. Between the impacts, motion of the second wheel is governed by a linear differential equation and can be analytically determined. Impacts are treated by modifying the initial conditions of motion, according to the Newton impact laws.

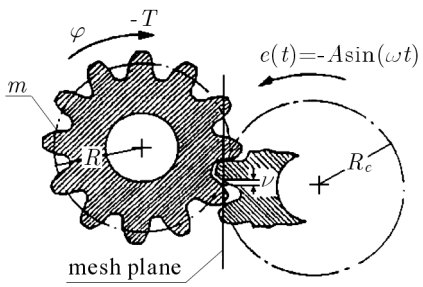

Fig. 1. Schematic view of a single-stage gearbox system

In an absolute coordinate system, we denote by φ the angular displacement of the second gear, such that the rotation dynamics is governed by the following equation of motion

$$m\varphi'' + \nu\varphi' = -T \tag{2.1}$$

where primes denote differentiation with respect to time, m is the moment of inertia, ν is the oil drag coefficient, and T is the oil splash torque.

The relative displacement between the gears due to the backlash is thus

$$s = \frac{AR_e}{\nu}\sin(\omega t) - \frac{R}{\nu}\varphi \tag{2.2}$$

in such a way that $-1 < s < 0$.

The equation of motion, in the relative coordinate system, is obtained from (2.1) and (2.2), resulting in

$$\ddot{s} + \beta\dot{s} = \ddot{e} + \beta\dot{e} + \gamma \tag{2.3}$$

where dots stand for derivatives with respect to the scaled time $\tau = \omega t$, and we have introduced the following non-dimensional parameters

$$\alpha \equiv \frac{AR_e}{\nu} \qquad \beta \equiv \frac{d}{m\omega} \qquad \gamma \equiv \frac{TR}{m\omega^2} \tag{2.4}$$

representing the damping coefficient, excitation amplitude, and moment of inertia, respectively.

Since equation (2.3) is linear, it can be integrated analytically between two impacts for the initial conditions $s(\tau_0) = s_0$, and $\dot{s}(\tau_0) = \dot{s}_0$. The displacement s and velocity $\dot{s}$ between impacts is given by

$$\begin{aligned} s(\tau) &= s_0 + \alpha(\sin\tau - \sin\tau_0) + \frac{\gamma}{\beta}(\tau - \tau_0) + \\ &\quad + \frac{1}{\beta}\{1 - \exp[-\beta(\tau - \tau_0)]\}\Big(\dot{s}_0 - \alpha\cos\tau_0 - \frac{\gamma}{\beta}\Big) \\ \dot{s}(\tau) &= \alpha\cos\tau + \Big(\dot{s}_0 - \alpha\cos\tau_0 - \frac{\gamma}{\beta}\Big)\exp[-\beta(\tau - \tau_0)] + \frac{\gamma}{\beta} \end{aligned} \tag{2.5}$$

An impact occurs whenever $s = -1$ or 0, since they actually correspond to the backlash boundaries. At these points, motion is no longer smooth and we have to reset the initial conditions according to the Newton laws of inelastic impact

$$\tau_0 = \tau \qquad s_0 = s \qquad \dot{s}_0 = -r\dot{s} \tag{2.6}$$

where $0 < r < 1$ is the restitution coefficient.

Adopting the instant of each collision as the time unit, we can define discrete variables s_n, $\dot{s}_n$, and τ_n representing the displacement, velocity, and time (*modulo* 2π) just before the n-th impact, respectively. Thanks to the analytical solution of the equations of motion between two impacts, we can substitute the initial conditions $\tau_0 = \tau_n$, $s_0 = s_n$, and $\dot{s}_0 = -r\dot{s}_n$ into Eqs. (2.5). With this representation we have a mapping relating the dynamical variables for the $n+1$-th impact to their corresponding values just before the n-th impact

$$\begin{aligned} s_{n+1} &= s_n + \alpha(\sin\tau_{n+1} - \sin\tau_n) + \frac{\gamma}{\beta}(\tau_{n+1} - \tau_n) + \\ &\quad - \frac{1}{\beta}\{1 - \exp[-\beta(\tau_{n+1} - \tau_n)]\}\Big(r\dot{s}_n + \alpha\cos\tau_n + \frac{\gamma}{\beta}\Big) \\ \dot{s}_{n+1} &= \alpha\cos\tau_{n+1} + \frac{\gamma}{\beta} - \exp[-\beta(\tau_{n+1} - \tau_n)]\Big(r\dot{s}_n + \alpha\cos\tau_n + \frac{\gamma}{\beta}\Big) \end{aligned} \tag{2.7}$$

This map is used here to calculate the Lyapunov exponents (de Souza and Caldas, 2004). Such exponents are computed through $\lambda_i = \lim_{n\to\infty}(1/n)\ln|\Lambda_i(n)|$, $(i = 1, 2)$, where $\Lambda_i(n)$ are the eigenvalues of the matrix $\mathbf{A} = \mathbf{J}_1\mathbf{J}_2\cdots\mathbf{J}_n$, where $\mathbf{J}_n$ is the Jacobian matrix of the map, computed at time n. For systems without analytical solutions between the impacts, the Lyapunov exponents can be calculated by using the methods proposed by Jin and co-workers (Jin *et al.*, 2006).

2.2. Fractal basin boundaries and chaotic transient

In Fig. 2, we show time series for the relative displacement $s(t)$ for three qualitatively different classes of behaviour: (i) one impact with the wall at $s = -1$ for two successive impacts with the wall at $s = 0$ (Fig. 2a); (ii) one impact with each wall (Fig. 2b); and (iii) one impact with the wall at $s = 0$ for two impacts with the wall at $s = -1$ (Fig. 2c).

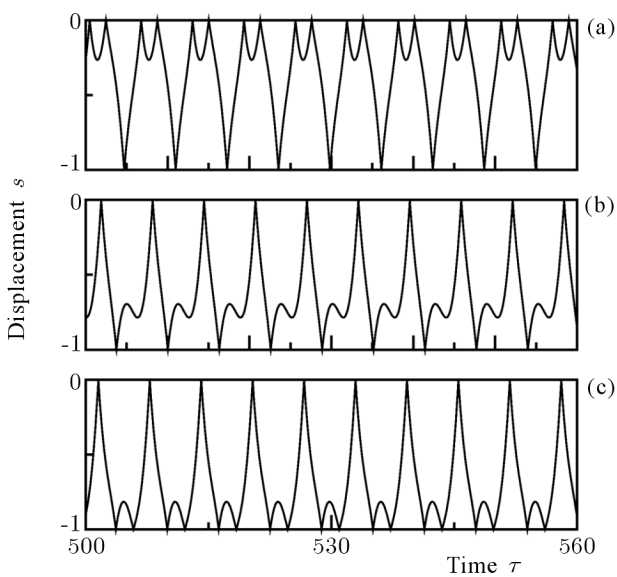

Fig. 2. Time histories of three co-existing attractors for amplitude excitation $\alpha = 0.5$ and restitution coefficient $r = 0.9$

The initial conditions leading to each of these behaviour scenarios are depicted in Fig. 3a with different shades of gray. Similarly as we define a basin of a given attractor as a set of initial conditions which generates trajectories asymptotically tending to this attractor, we may call the sets in Fig. 3a as *basins of behaviour*, with the same interpretation. The basins of each behaviour

are densely mixed and, as suggested by the magnification shown in Fig. 3b, the basin boundary looks like a fractal curve.

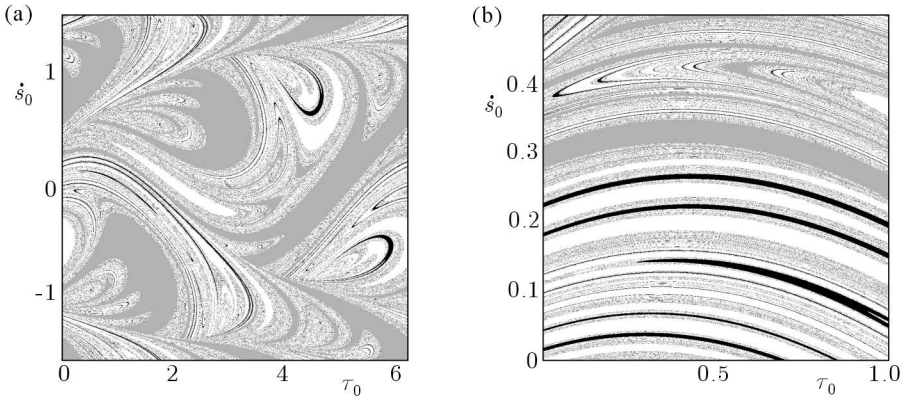

Fig. 3. (a) Basins of behaviour for three co-existing attractors shown in Figs. 2a-c. (b) Magnification of the previous figure

The boundary between the behaviour basins in Fig. 3 is indeed fractal, which is quantitatively confirmed by Fig. 4, where we show variation of the uncertain fraction $f(\epsilon)$ of the phase space section shown in Fig. 3 as a function of the uncertainty radius ϵ. By *uncertain fraction* we mean the result of the following numerical experiment: we create a fine mesh of initial conditions in the plane $(\dot{s}_n, \tau_n)$ and consider the fate of a trajectory starting from each initial condition and another, very close, initial condition far apart from the former by a distance ϵ. If both trajectories tend asymptotically to different final responses, the initial condition is said to be ϵ-uncertain (McDonald *et al.*, 1983, 1985).

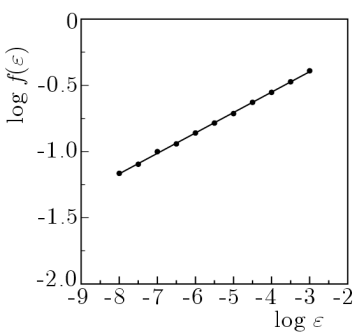

Fig. 4. Uncertain fraction *versus* uncertainty radius ϵ for basins of behaviour showed in Fig. 3. The solid curve is a linear regression fit with slope $\varpi = 0.154 \pm 0.001$

The uncertain fraction is the relative number of ϵ-uncertain initial conditions. We expect from general arguments that this fraction scales with the uncertainty radius as a power law: $f(\epsilon) \sim \epsilon^{\varpi}$, where $\varpi = 2 - d_B$ is called the uncertainty exponent, d_B being the box-counting dimension of the basin boundary. If $0 < \varpi < 1$ then $1 < d_B < 2$ and the basin boundary is a fractal curve. As shown in Fig. 4, this scaling is verified for this case where a least-squares fit shows that $\varpi = 0.154 \pm 0.001$, confirming that the basin boundary is a fractal with final-state sensitivity. As an illustration of the consequences of this fractality, suppose one manages to diminish the uncertainty radius by a factor of ten. Due to the small value of the uncertainty exponent ϖ, the corresponding decrease in the uncertain fraction is a factor $\sim 10^{-0.15} \approx 0.708$ only.

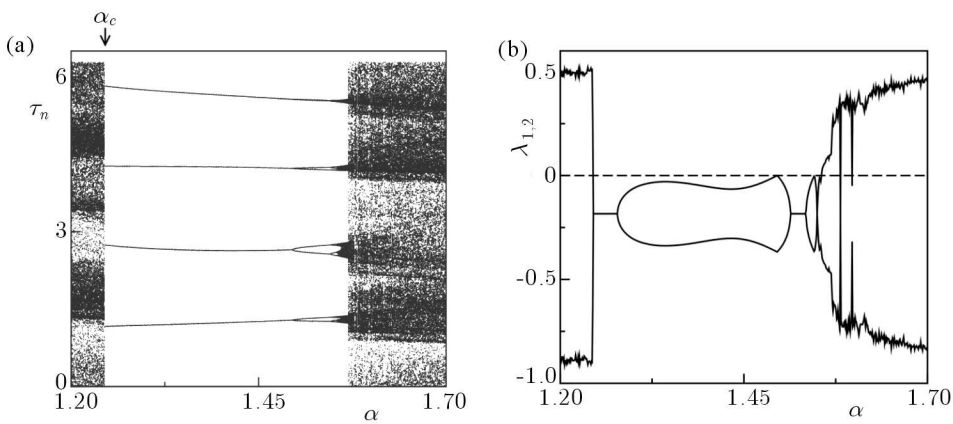

Fig. 5. (a) Bifurcation diagram of the impact moment τ_n as a function of the excitation amplitude α for $R = 0.9$. (b) Lyapunov exponents $\lambda_{1,2}$ as a function of α

In Fig. 5a we plot a bifurcation diagram showing the asymptotic values of the variable τ_n *versus* the excitation amplitude α. The interesting feature of this diagram is that the chaotic behaviour of τ_n is suppressed as the damping increases, as would be expected from general arguments. However, this change does not occur smoothly but rather in an abrupt way, after a crisis at $\alpha_C \approx 1.25$ leading to a stable period-1 orbit corresponding to four impacts (two with each wall) (de Souza *et al.*, 2004). The latter is followed by a period-doubling bifurcation cascade and a wide chaotic region for higher damping, a surprising fact. Figure 5b shows the corresponding diagram for the Lyapunov exponents.

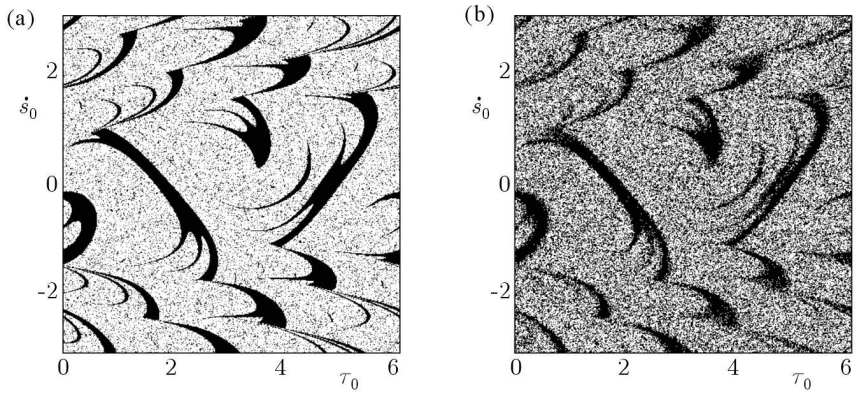

Fig. 6. Basins of transient behaviour with $\alpha = 1.245$ for noise levels (a) $\sigma = 0$, and (b) $\sigma = 0.03$

Figure 6 illustrates the effect of additive noise in the basin boundary structure of the gearbox system (de Souza *et al.*, 2005b). The additive noise is here represented by a pseudo-random variable with uniform distribution and noise level σ. We fixed a number, say 500 iterations of the gearbox system, and consider whether or not the evolution is chaotic. The behaviours indicated in Fig. 6 is the following: (i) periodic evolution (black pixels); (ii) chaotic transient evolution (white pixels). For zero noise (Fig. 6a) the transient basins are already mixed up but, as we switch on the external noise, most of the basins are related to the periodic attractor (Fig. 6b). This decrease of the relative area of the chaotic transient basin can be measured as a function of the noise level. Our results support a linear decay law: $0.708 - 8.176\sigma$ (Fig. 7).

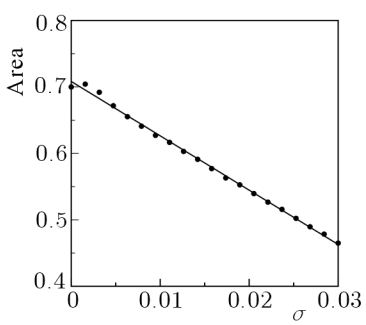

Fig. 7. Relative area A of the chaotic transient basin as a function of noise perturbation σ. The solid curve is a linear regression fit

3. Controlling chaos in vibro-impact systems

Since chaotic motion is quite common in vibro-impact systems, leading to sometimes undesirable effects, it is important to devise methods to control chaotic motion (Bishop *et al.*, 1998; Fradkov *et al.*, 2006; Lee and Yan, 2006). In 1990, a scheme of chaos control was put forward by Ott, Grebogi and Yorke (Ott *et al.*, 1990). The so-called *OGY method* consists on stabilizing a desired unstable periodic orbit embedded in a chaotic attractor by using only a tiny perturbation on an available control parameter. Another interesting chaos control strategy was proposed in (Pyragas, 1992) who also considered dynamical properties of a chaotic attractor to stabilize unstable periodic orbits. In that case the method implementation required a delayed feedback signal. Another kind of feedback control method was proposed in recent years (Alvarez-Ramirez *et al.*, 2003; Tereshko *et al.*, 2004), using a small-amplitude control signal, applied to alter the energy of a chaotic system. We used another approach, namely to alter the damping coefficient, to suppress chaotic motion and steer the system to some desired periodic attractor (de Souza *et al.*, 2007a).

3.1. Impact oscillator

We applie a control strategy in order to suppress chaotic motion in a vibro-impact system. Figure 8 depicts a model of an impact oscillator, which is a periodically forced and damped linear one-dimensional oscillator whose displacement is limited by an amplitude constraint, a fixed wall at $x = x_c$. Between two successive impacts, smooth motion without control input, is given by

$$\ddot{x} + c\dot{x} + x = \alpha\cos(\omega t) \tag{3.1}$$

where c is the damping coefficient, F is the forcing amplitude, and ω is the forcing frequency. Both the oscillator mass and the elastic constant have been normalized to unity for simplicity.

Considering the control method by de Souza *et al.* (2007a), the equation of motion is described by

$$\ddot{x} + f_d(\dot{x}) + x = \alpha\cos(\omega t) \tag{3.2}$$

where

$$f_d(\dot{x}) = \begin{cases} (c-k)\dot{x} & \text{if} \quad \dot{x} \geqslant 0 \\ c\dot{x} & \text{if} \quad \dot{x} < 0 \end{cases}$$

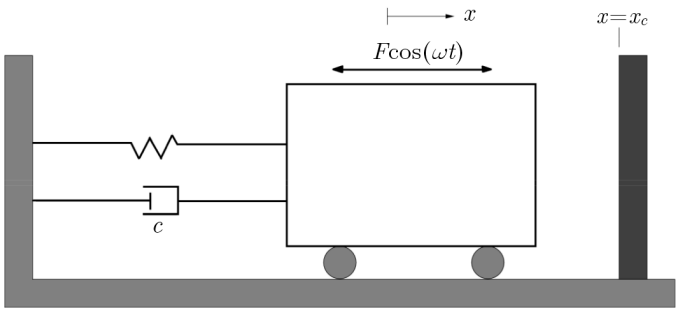

Fig. 8. Model of an impact oscillator

and k is a constant coefficient. In this case, the damping coefficient is decreased for positive velocities and is not changed for negative velocities.

An impact occurs whenever $x = x_c$. After each impact, we reset the velocity of the oscillator using Newton's impact law. In other words, we model the collisions with a rigid wall (amplitude constraint) by the law of inelastic impact: the velocity after the impact is taken to be $-r$ times the velocity before the impact, where r is a constant restitution coefficient $(0 < r < 1)$.

3.2. Suppressing chaotic vibrations

Numerical simulations were performed by using the fourth-order Runge-Kutta method. We adopted a fixed step for displacements far away from the rigid wall (amplitude constraint) and an adaptive step, if we are close enough to the wall. The adaptive step was obtained using the Newton-Raphson method. The control parameter values were fixed at $x_c = 0$, $r = 0.8$, $\alpha = 2.0$, and $\omega = 2.8$.

For the control switched off, in Fig. 9a, we show a bifurcation diagram of the velocity $\dot{x}$ just before an impact with the amplitude constraint in terms of the damping coefficient c. Hence, as can be seen, there is a wide range of the parameter for which the system presents chaotic attractors, with one and two bands, occasionally interrupted by narrow periodic windows.

In order to verify the performance of the control method, we present in Fig. 9b, for $c = 0.7$, a bifurcation diagram in terms of the parameter k, that is associated with the damping coefficient, showing the transformation of the chaotic attractor for small k into a period-1 orbit as k is increased from zero through a reverse period-doubling bifurcation cascade. From these results, by varying the damping coefficient according to velocities, we can obtain the suppression of chaotic regimes.

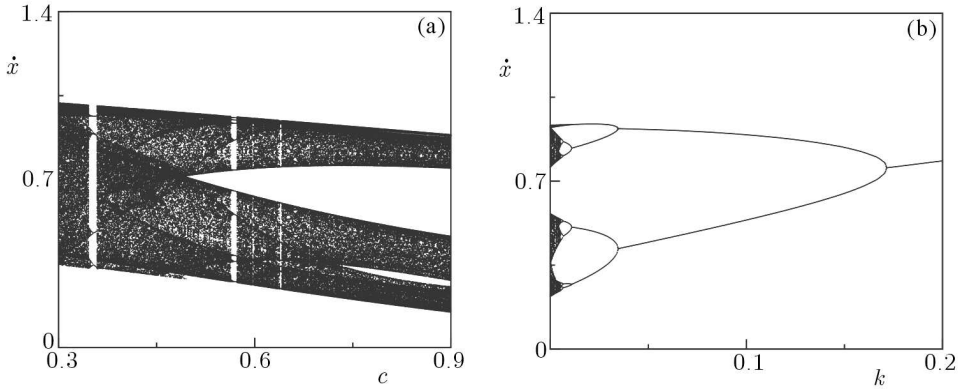

Fig. 9. Bifurcation diagrams of the velocity just before the impact as a function of (a) damping parameter c for $k = 0$; and (b) control parameter k for $c = 0.7$

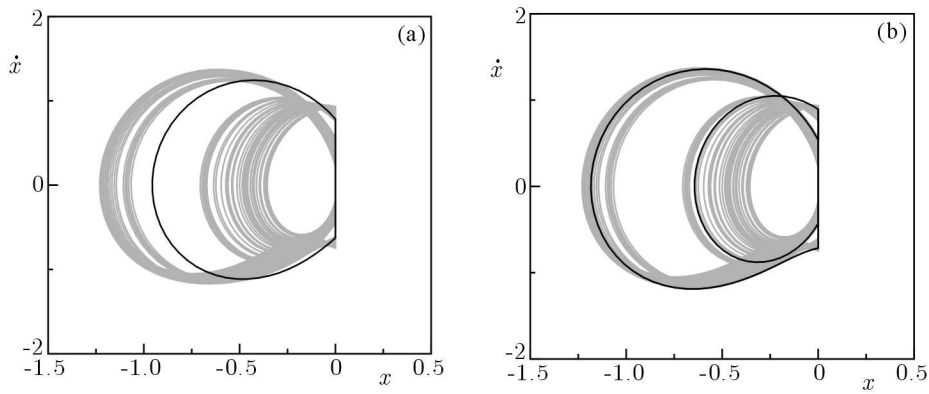

Fig. 10. Phase portraits for $c = 0.7$ and (a) $k = 0.2$; (b) $k = 0.1$. The uncontrolled chaotic attractor $(k = 0)$ is depicted in the background

In Fig. 10a we show an example of the suppression of chaotic regimes, where we plot the phase portrait, for $c = 0.7$, of the period-1 orbit that was obtained for $k = 0.2$. In the background of this figure, a chaotic attractor without control $(k = 0)$ is depicted. When k is changed to a smaller value, the resulting orbit has period 2, Fig. 10b. We present in Fig. 11 an example of the control implementation for this case, where we depict the evolution of velocity collected just before the impacts as a function of the impact number n. The control is switched on at the time $n = 1000$ for $k = 0.1$ and a period-2 orbit is obtained. At $n = 2000$ the control is switched off and at $n = 3000$ it is switched on again, for $k = 0.025$, after which we obtain a period-4 orbit.

At $n = 4000$ the control is switched off and, finally, at $n = 5000$ the control is switched on again for $k = 0.2$, resulting in the period-1 orbit shown in Fig. 3a.

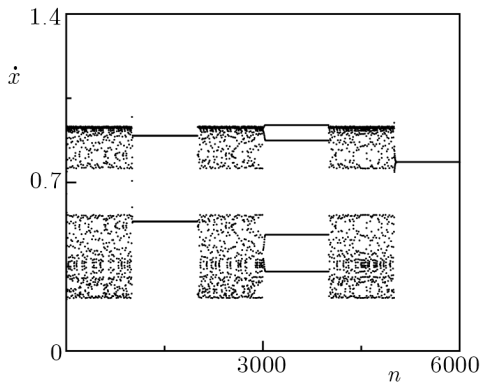

Fig. 11. Time series of the velocity just before an impact as a function of the impact number n for $c = 0.7$ and the application of control at three time instants (see text for details)

4. Oscillator with limited power supply

Most studies of driven oscillators assume that the driving comes from an external source which is not appreciably perturbed by motion of the oscillator (ideal systems). However, in practical situations, the dynamics of the forcing system cannot be considered as given *a priori*, and it must be taken as also a consequence of the dynamics of the whole system (Kononenko, 1969). In other words, the forcing system has a limited energy source as that provided by an electric motor for example, and thus its own dynamics is influenced by that of the oscillating system being forced (Krasnopolskaya and Shvets, 1993). This increases the number of degrees of freedom, and is called a non-ideal problem.

In terms of the vibrating cart model, the non-ideal system is obtained by replacing the external sinusoidal driving of the cart by the rotor attached to the cart, and fed by the motor (Warminski *et al.*, 2001). The angular momentum of the rotor is imparted to the cart. The application of non-ideal models to some vibro-impact problems has been considered in recent papers (Dimentberg *et al.*, 1997; de Souza *et al.*, 2005a, 2007b; Xu *et al.*, 2007).

4.1. Non-ideal oscillator

We consider one-dimensional motion of a cart of the mass M (mass considering the motor) connected to a fixed frame by a nonlinear spring and a dash-pot (viscous coefficient c), as shown in Fig. 12. The nonlinear spring stiffness is given by $k_1X - k_2X^3$, where X denotes the cart displacement. Motion of the cart is due to an in-board non-ideal motor driving the rotor. We denote by φ the angular displacement of the rotor with the mass m_0 and a massless rod of radius R.

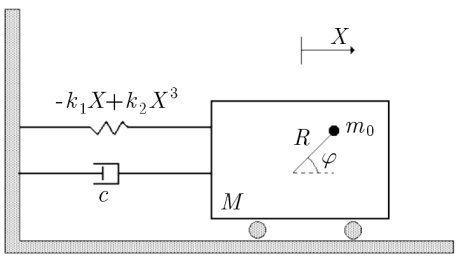

Fig. 12. Schematic model of a non-ideal oscillator

It is convenient to work with dimensionless dynamical variables, according to the following definitions

$$x \equiv \frac{X}{R} \qquad \tau \equiv t\sqrt{\frac{k_1}{M}} \tag{4.1}$$

The equations of motion for both the cart and the rotor are given, respectively, by

$$\begin{aligned} &\ddot{x} + \beta\dot{x} - x + \delta x^3 = \epsilon_1(\ddot{\varphi}\sin\varphi + \dot{\varphi}^2\cos\varphi) \\ &\ddot{\varphi} - \epsilon_2\cos\varphi = \ddot{x}\sin\varphi + E_1 - E_2\dot{\varphi} \end{aligned} \tag{4.2}$$

where the dots stand for differentiation with respect to the scaled time τ, and the following abbreviations were introduced

$$\beta \equiv \frac{c}{\sqrt{k_1 M}} \qquad \delta \equiv \frac{k_2}{k_1}R^2 \qquad \epsilon_1 \equiv \frac{m_0}{M} \qquad \epsilon_2 \equiv \frac{g}{Rk_1} \tag{4.3}$$

The parameters E_1 and E_2 can be estimated from the characteristic curve of the energy source (DC-motor).

4.2. Co-existence of attractors

Numerical simulations of nonlinear oscillator systems were performed by using the fourth-order Runge-Kutta method with a fixed step. The system parameters were fixed at $\beta = 0.02$, $\delta = 0.1$, $\epsilon_1 = 0.1$, $\epsilon_2 = 1.0$, and $E_2 = 1.5$. As representative examples of typical solutions obtained for the considered non-ideal oscillator model, we show in Fig. 13a a bifurcation diagram for the displacement *versus* the parameter E_1. In this figure, we identify the co-existence of attractors, both periodic (of various periods) and chaotic. For example, three periodic attractors are observed for $E_1 = 2.0$ (the point labelled as C in Fig. 13a), one periodic and one chaotic attractor for $E_1 = 2.5$ (the points labelled as A and B in Fig. 13a), and two quasi-periodic and one periodic attractor at $E_1 = 4.0$ (the point labelled as D in Fig. 13a). In Fig. 13b, we depict the same bifurcation diagram for the Lyapunov exponents of the attractor labelled as A in Fig. 13a. We used the algorithm of (Wolf *et al.*, 1985) to numerically obtain the Lyapunov exponents for this model.

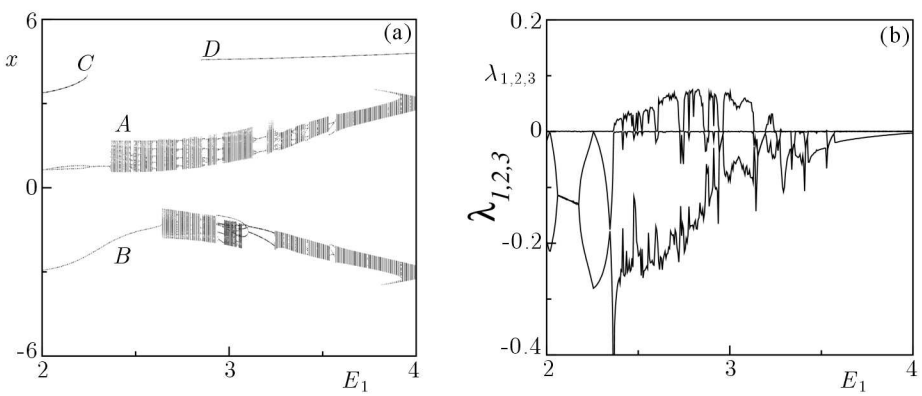

Fig. 13. (a) Bifurcation diagram for the cart displacement *versus* the control parameter E_1 showing the co-existence of attractors. (b) Three largest Lyapunov exponents of attractors A

The situation where the chaotic attractor A coexists with the periodic attractor B (Fig. 14) deserves particular attention. Depending on the initial condition chosen, the trajectory will asymptote to one or another attractor. Curiously, both attractors correspond to oscillations with similar ranges both in the position and velocity of the cart. The basins of attractions of both attractors have a quite complicated structure, as shown in Fig. 15, where the initial conditions converging to the chaotic (periodic) attractor are depicted with white (dark gray) pixels. Using the uncertain fraction approach outlined in Section 2, we computed the dependence of the uncertain fraction with the

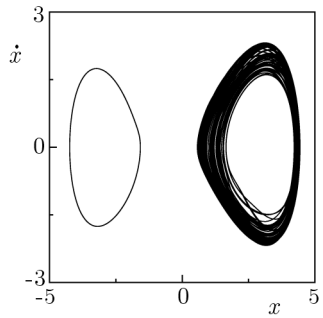

Fig. 14. Phase portraits for the control parameter $E_1 = 2.5$ showing the co-existence of periodic and chaotic attractors

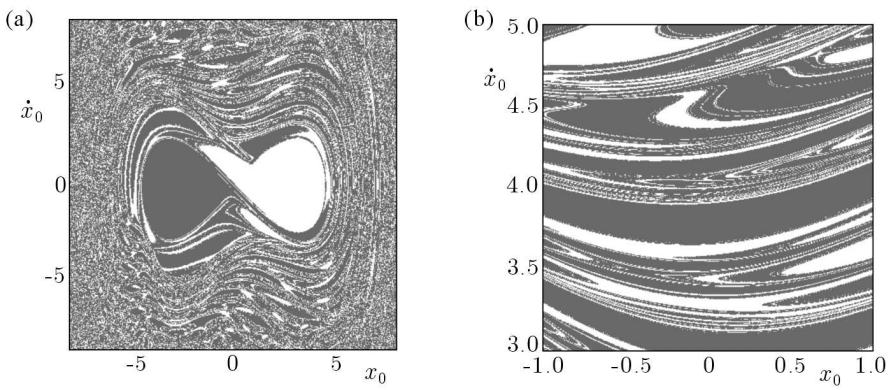

Fig. 15. (a) Basins of attraction for the two co-existing attractors shown in Fig. 14. (b) Magnification of the previous figure

uncertainty radius, obtaining a power-law scaling with the exponent $\varpi = 0.445 \pm 0.008$, corresponding to the fractal basin boundary with box-counting dimension $d_B = 1.555$ (Fig. 16).

5. Non-ideal oscillator with a tube liquid damper

The need to mitigate wind, ocean wave and earthquake induced vibrations in structures like tall buildings, long span bridges and offshore platforms has led to a steadfast interest in damping devices. Impact dampers are a very useful way to suppress unwanted high-amplitude vibrations in small-scale systems, but they are somewhat difficult, if not impossible, to implement in large-scale engineering structures (Chaterjee *et al.*, 1995). For the latter systems, tuned

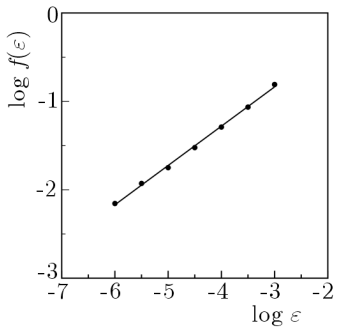

Fig. 16. Uncertain fraction in the phase space region shown in Fig. 15b *versus* the uncertainty radius ϵ. The solid curve is a linear regression fit with slope $\varpi = 0.445 \pm 0.008$

liquid dampers (TLDs) and tuned liquid column dampers (TLCDs) have gained special attention by virtue of their simplicity and flexibility (Yalla and Kareem, 2001). A tuned liquid damper is basically a mass-spring-dashpot system connected to the structure and works due to the inertial secondary system principle by which the damper counteracts the forces producing vibration (Yalla *et al.*, 2001; Felix *et al.*, 2005).

A tuned liquid column damper replaces the mass-spring-dashpot system by a U-tube-like container where motion of a liquid column absorbs a part of the vibration on the system with a valve/orifice playing the role of damping. A TLCD has an additional advantage of being a low-cost application. In a tall building, for example, the container can also be used as a building water supply, whereas in a TLD, the mass-spring-dashpot is a dead-weight component without further use. In fact, vibration control through TLCD has been recently used in other engineering applications, such as ship and satellite stabilization. Whereas the damping characteristic of a mass-spring-dashpot system of a TLD is essentially linear, the damping in a liquid column is amplitude-dependent (regulated by the orifice in the bottom of the U-tube) and consequently nonlinear. Hence, the dynamics of a TLCD is far from being simple, and very few analytical results can be obtained. Numerical explorations of dynamics of a TLCD mounted on a structural frame, using a non-ideal motor as a source of energy, have been performed recently (Felix *et al.*, 2005).

The liquid damper consists of a U-shaped tube attached to the top of the cart, containing a liquid of the total mass m and density ρ, Fig. 17 (de Souza *et al.*, 2006). The distance between the two vertical columns is denoted by b and the distance of the liquid levels in these columns will be denoted by l. The vertical displacement of the left column with respect to the liquid level, when

the cart is at rest, is denoted by Y. There is a valve at the middle point of the tube bottom whose aperture can be tuned in order to vary the resistance to the flow through this orifice. This is the source of the nonlinear and amplitude-dependent damping experienced by the liquid mass while flowing through the U-tube. The coefficient of head loss of the valve is ξ.

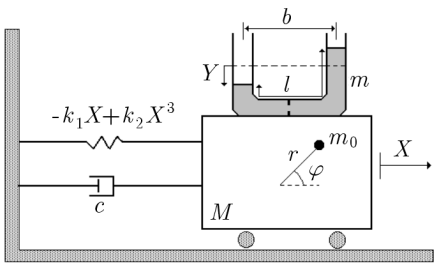

Fig. 17. Non-ideal system with a liquid damper

Motion of the combined cart-liquid damper system is governed by the following equations

$$\begin{aligned}
&(1+\mu)\ddot{x} + \beta\dot{x} - x + \delta x^3 = \epsilon_1(\ddot{\varphi}\sin\varphi + \dot{\varphi}^2\cos\varphi) - \alpha_1\mu\ddot{y}\\
&\ddot{\varphi} + \epsilon_2\cos\varphi = \ddot{x}\sin\varphi + E_1 - E_2\dot{\varphi}\\
&\ddot{y} + \gamma|\dot{y}|\dot{y} + \sigma y = \alpha_1\ddot{x}
\end{aligned} \tag{5.1}$$

where

$$\mu \equiv \frac{m}{M} \qquad \gamma \equiv \frac{\xi r}{2l} \qquad \sigma \equiv \frac{k_3}{k_1\mu} \qquad \alpha_1 \equiv \frac{b}{l} \tag{5.2}$$

Figure 18 shows phase portraits for the oscillator without (in gray) and with the damper (in black). In the uncontrolled case, we have coexistence of the periodic and chaotic attractor. As can be seen, considering the controller, the amplitudes of periodic and chaotic vibrations are decreased, and the chaotic attractor is suppressed. The parameters of the damper are fixed at $\alpha_1 = 3.0$, $\gamma = 0.4$, $\sigma = 1.0$, and $\mu = 0.01$. The basin structure in this situation is shown in Fig. 19, showing a quite complicated structure of interrupted striations. However, it should be noted that the basins here are simpler than in the case analysed in Fig. 15 for a non-ideal system.

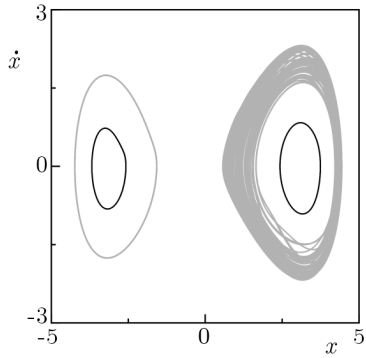

Fig. 18. Phase portraits for the control parameter $E_1 = 2.5$ showing the co-existence of periodic and chaotic attractors without control (in gray); and two periodic attractors with the liquid damper (black), for $\alpha = 3.0$, $\gamma = 0.4$, $\sigma = 1.0$, and $\mu = 0.01$

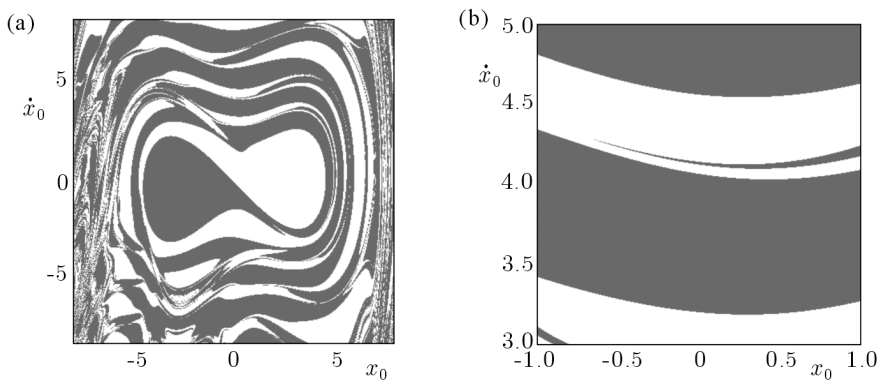

Fig. 19. (a) Basins of attraction for the two co-existing attractors (in black) shown in Fig. 18. (b) Magnification of the previous figure

6. Conclusions

In this paper, we reviewed some recent works authors have done on complex dynamics in vibro-impact systems, focusing chiefly on chaotic motion and its control through different schemes. Besides their evident engineering applications, vibro-impact systems enjoy also a more fundamental interest due to the loss of smoothness in their dynamics, leading to a plethora of complex dynamical phenomena, some of them being presented throughout this paper. We have seen that in all systems considered, chaotic motion is a ubiquitous feature, presenting some challenging questions concerning to its control or suppression.

As an example of vibro-impact systems, we considered a gear box model and discussed the coexistence of attractors with fractal basin boundaries as well as the existence of long chaotic transients. In addition, we used smart dampers to suppress chaotic vibrations of an impact oscillator.

Another feature considered in this paper is taking into account the finiteness of oscillator energy sources. As an example of a non-ideal system, we analysed chaotic dynamics of the damped Duffing oscillator coupled to a rotor. For that system, we identified the influence of the power supply on attractors. Moreover, we showed how to use a tuned liquid damper to control the attractors of such a non-ideal oscillator.

In conclusion, we presented examples of controlling chaotic dynamics of vibro-impact and non-ideal oscillators. The used control procedure may help avoiding undesirable behaviour of mechanical systems with practical applications.

Acknowledgements

This work has been made possible by partial financial support from the following Brazilian government agencies: FAPESP, CNPq, and Capes. The authors would like to thank Professor Tomasz Kapitaniak for his continuous encouragement and valuable discussions and suggestions.

References

1. Alvarez-Ramirez J., Espinosa-Paredes G., Puebla H., 2003, Chaos control using small-amplitude damping signals, *Physics Letters A*, **316**, 196-205

2. Bishop S.R., Wagg D.J., Xu D., 1998, Use of control to maintain period-1 motions during wind-up or wind-down operations of an impacting driven beam, *Chaos, Solitons and Fractals*, **9**, 261-269

3. Blazejczyk-Okolewska B., Czolczynski K., Kapitaniak T., Wojewoda J., 1999, *Chaotic Mechanics in Systems with Friction and Impacts*, World Scientific, Singapore

4. Blazejczyk-Okolewska B., Czolczynski K., Kapitaniak T., 2004, Classification principles of types of mechanical systems with impacts – fundamental assumptions and rules, *European Journal of Mechanics – A/Solids*, **23**, 3, 517-537

5. Chaterjee S., Mallik A.K., Ghosh A., 1995, On impact dampers for nonlinear vibrating systems, *Journal of Sound and Vibration*, **187**, 403-420

6. Czolczynski K., Blazejczyk-Okolewska B., Kapitaniak T., 2000, Impact force generator: self-synchronization and regularity of motion, *Chaos, Solitons and Fractals*, **11**, 2505-2510

7. de Souza S.L.T., Caldas I.L., 2001, Basins of attraction and transient chaos in a gear-rattling model, *Journal of Vibration and Control*, **7**, 849-862

8. de Souza S.L.T., Caldas I.L., 2004, Calculation of Lyapunov exponents in systems with impacts, *Chaos, Solitons and Fractals*, **19**, 569-579

9. de Souza S.L.T., Caldas I.L., Viana R.L., Balthazar J.M., 2004, Sudden changes in chaotic attractors and transient basins in a model for rattling in gearboxes, *Chaos, Solitons and Fractals*, **21**, 763-772

10. de Souza S.L.T., Caldas I.L., Viana R.L., Balthazar J.M., Brasil R.M.L.R.F., 2005a, Basins of attraction changes by amplitude constraining of oscillators with limited power supply, *Chaos, Solitons and Fractals*, **26**, 1211-1220

11. de Souza S.L.T., Caldas I.L., Viana R.L., Batista A.M., Kapitaniak T., 2005b, Noise-induced basin hopping in a gearbox model, *Chaos, Solitons and Fractals*, **26**, 1523-1531

12. de Souza S.L.T., Caldas I.L., Viana R.L., Balthazar J.M., Brasil R.M.L.R.F., 2006, Dynamics of vibrating systems with tuned liquid column dampers and limited power supply, *Journal of Sound and Vibration*, **289**, 987-998

13. de Souza S.L.T., Caldas I.L., Viana R.L., 2007a, Damping control law for a chaotic impact oscillator, *Chaos, Solitons and Fractals*, **32**, 745-750

14. de Souza S.L.T., Caldas I.L., Viana R.L., Balthazar J.M., Brasil R.M.L.R.F., 2007b, A simple feedback control for a chaotic oscillator with limited power supply, *Journal of Sound and Vibration*, **299**, 664-671

15. de Souza S.L.T., Wiercigroch M., Caldas I.L., Balthazar J.M., 2007c, Suppressing grazing chaos in impacting system by structural nonlinearity, *Chaos, Solitons and Fractals*, in press, doi:10.1016/j.chaos.2007.01.022

16. Dimentberg M.F., McGovern L., Norton R.L., Chapdelaine J., Harrison R., 1997, Dynamics of an unbalanced shaft interacting with a limited power supply, *Nonlinear Dynamics*, **13**, 171-187

17. Felix J.L.P., Balthazar J.M., Brasil R.M.L.R.F., 2005, On tuned liquid column dampers mounted on a structural frame under a non-ideal excitation, *Journal of Sound and Vibration*, **282**, 1285-1292

18. Fradkov A.L., Evans R.J., Andrievksy B.R., 2006, Control of chaos: methods and applications in mechanics, *Philosophical Transactions of The Royal Society A*, **364**, 2279-2307

19. Ing J., Pavlovskaia E., Wiercigroch M., 2006, Dynamics of a nearly symmetrical piecewise linear oscillator close to grazing incidence: modelling and experimental verification, *Nonlinear Dynamics*, **46**, 225-238

20. Ivanov A.P., 1996, Bifurcations in impact systems, *Chaos, Solitons and Fractals*, **7**, 1615-1634

21. Jerrelind J., Stensson A., 2000, Nonlinear dynamics of parts in engineering systems, *Chaos, Solitons and Fractals*, **11**, 2413-2428

22. Jin L., Lu Q.S., Twizell E.H., 2006, A method for calculating the spectrum of Laypunov exponents by local maps in non-smooth impact-vibrating systems, *Journal of Sound and Vibration*, **298**, 1019-1033

23. Kapitaniak T., 2000, *Chaos for Engineers*, Springer Verlag, New York-Berlin-Heidelberg

24. Karagiannis K., Pfeiffer F., 1991, Theoretical and experimental investigations of gear-rattling, *Nonlinear Dynamics*, **2**, 367-387

25. Kononenko V.O., 1969, *Vibrating Systems with a Limited Power Supply*, Iliffe Books Ltd, London

26. Krasnopolskaya T.S., Shvets A.Y., 1993, Chaos in vibrating systems with a limited power-supply, *Chaos*, **3**, 387-395

27. Lee J.Y., Yan J.J., 2006, Control of impact oscillator, *Chaos, Solitons and Fractals*, **28**, 136-142

28. Luo A.C.J., 2004, Period-doubling induced chaotic motion in the LR model of a horizontal impact oscillator, *Chaos, Solitons and Fractals*, **19**, 823-839

29. Luo G.W., Chu Y.D., Zhang Y.L., Zhang J.G., 2006, Double Neimark-Sacker bifurcation and torus bifurcation of a class of vibratory systems with symmetrical rigid stops, *Journal of Sound and Vibration*, **298**, 154-179

30. Luo G.W., Zhang Y.L., Chu Y.D., Zhang J.G., 2007, Codimension-two bifurcations of fixed points in a class of vibratory systems with symmetrical rigid stops, *Nonlinear Analysis: Real World Applications*, **8**, 1272-1292

31. McDonald S.W., Grebogi C., Ott E., 1983, Final state sensitivity: an obstruction to predictability, *Physics Letters A*, **99**, 415-418

32. McDonald S.W., Grebogi C., Ott E., 1985, Fractal basin boundaries, *Physica D*, **17**, 125-153

33. Nordmark A.B., 1991, Non-periodic motion caused by grazing incidence in an impact oscillator, *Journal of Sound and Vibration*, **145**, 279-297

34. Ott E., Grebogi C., Yorke J.A., 1990, Controlling chaos, *Physical Review Letters*, **64**, 1196-1199

35. Pavlovskaia E., Wiercigroch M., Grebogi C., 2001, Modeling of an impact system with a drift, *Physical Review E*, **64**, 056224

36. PETERKA F., VACIK J., 1992, Transition to chaotic motion in mechanical systems with impacts, *Journal of Sound and Vibration*, **154**, 95-115

37. PFEIFFER F., KUNERT A., 1990, Rattling models from deterministic to stochastic processes, *Nonlinear Dynamics*, **1**, 63-74

38. PYRAGAS K., 1992, Continuous control of chaos by self-controlling feedback, *Physics Letters A*, **170**, 421-428

39. TERESHKO V., CHACÓN R., PRECIADO V., 2004, Controlling chaotic oscillators by altering their energy, *Physics Letters A*, **320**, 408-416

40. WARMINSKI J., BALTHAZAR J.M., BRASIL R.M.L.R.F., 2001, Vibrations of a non-ideal parametrically and self-excited model, *Journal of Sound and Vibration*, **245**, 363-374

41. WIERCIGROCH M., 2000, Modelling of dynamical systems with motion dependent discontinuities, *Chaos, Solitons and Fractals*, **11**, 2429-2442

42. WIERCIGROCH M., DE KRAKER B., 2000, *Applied Nonlinear Dynamics and Chaos of Mechanical Systems with Discontinuities*, World Scientific, Singapore

43. WIERCIGROCH M., WOJEWODA J., KRIVTSON A.M., 2005, Dynamics of ultrasonic percussive drilling of hard rocks, *Journal of Sound and Vibration*, **280**, 739-757

44. WOLF A., SWIFT J.B., SWINNEY H.L., VASTANO J.A., 1985, Determining Lyapunov exponents from a time series, *Physica D*, **16**, 285-317

45. XU X., PAVLOVSKAIA E., WIERCIGROCH M., ROMEO F., LENCI S., 2007, Dynamic interactions between parametric pendulum and electro-dynamical shaker, *Z. Angew. Math. Mech.*, **87**, 172-186

46. YALLA S.K., KAREEM A., 2001, Beat phenomenon in combined structure-liquid damper systems, *Engineering Structures*, **23**, 622-630

47. YALLA S.K., KAREEM A., KANTOR J.C., 2001, Semi-active tuned liquid column dampers for vibration control of structures, *Engineering Structures*, **23**, 1469-1479

Sterowanie i chaos w układach drgających z uderzeniami oraz nieidealnych oscylatorów

Streszczenie

W pracy przedyskutowano zagadnienie dynamiki mechanizmów dwóch rodzajów. Najpierw rozważono układ drgający z uderzeniami, który znajduje liczne aplikacje praktyczne w mechanice stosowanej, począwszy od urządzeń wiertniczych przez procesy cięcia metalu do skrzyń biegów włącznie. Z punktu widzenia dynamiki maszyn

układy wibro-uderzeniowe wykazują bogactwo interesujących zjawisk, wliczając w to chaos. W pracy zaprezentowano przegląd ostatnich prac dotyczących dynamiki układów wibro-uderzeniowych, w których zajęto się problemem chaosu i możliwości jego sterowania. Przeanalizowano układy mechaniczne na przykładzie modelu kół zębatych z systemem "inteligentnego" tłumika do eliminacji ruchu chaotycznego. Zajęto się, po drugie, mechanizmami z nieidealnym źródłem energii odwzorowanym poprzez układ ograniczonego poboru mocy. Jako przykład zbadano dynamikę chaotyczną tłumionego oscylatora Duffinga połączonego z wirnikiem. Pokazano sposób zastosowania płynnego tłumika do sterowania formą atraktorów obserwowanych w nieidealnym oscylatorze.

Manuscript received December 17, 2007; accepted for print March 19, 2008